Verification of a new NOAA/NSIDC passive microwave sea-ice concentration climate record

Walter N. Meier,[1] Ge Peng,[2,3] Donna J. Scott[4] & Matt H. Savoie[4]

[1] Cryospheric Sciences Lab, Code 615, National Aeronautics and Space Administration Goddard Space Flight Center, Greenbelt, MD 20771, USA
[2] Cooperative Institute for Climate and Satellites, North Carolina State University, Raleigh, NC, USA
[3] Remote Sensing and Applications Division, National Oceanic and Atmospheric Administration National Climatic Data Center, 151 Patton Avenue, Asheville, NC 28801, USA
[4] National Snow and Ice Data Center, University of Colorado, UCB 449, Boulder CO 80309, USA

Abstract

A new satellite-based passive microwave sea-ice concentration product developed for the National Oceanic and Atmospheric Administration (NOAA) Climate Data Record (CDR) programme is evaluated via comparison with other passive microwave-derived estimates. The new product leverages two well-established concentration algorithms, known as the NASA Team and Bootstrap, both developed at and produced by the National Aeronautics and Space Administration (NASA) Goddard Space Flight Center (GSFC). The sea-ice estimates compare well with similar GSFC products while also fulfilling all NOAA CDR initial operation capability (IOC) requirements, including (1) self-describing file format, (2) ISO 19115-2 compliant collection-level metadata, (3) Climate and Forecast (CF) compliant file-level metadata, (4) grid-cell level metadata (data quality fields), (5) fully automated and reproducible processing and (6) open online access to full documentation with version control, including source code and an algorithm theoretical basic document. The primary limitations of the GSFC products are lack of metadata and use of untracked manual corrections to the output fields. Smaller differences occur from minor variations in processing methods by the National Snow and Ice Data Center (for the CDR fields) and NASA (for the GSFC fields). The CDR concentrations do have some differences from the constituent GSFC concentrations, but trends and variability are not substantially different.

Sea ice is an important climate change indicator. Changes in sea-ice extent and concentration reflect changes in air and ocean temperature as well as circulation patterns. Sea ice plays a key role in polar climate by reflecting incoming solar radiation during the summer and insulating the warmer ocean from the cold atmosphere during winter. It is a platform for numerous flora and fauna, from microscopic organisms to charismatic megafauna. In the Arctic, sea ice is a central component of the culture and life of indigenous people.

One of the most effective methods to track changes in sea ice is via satellite-borne passive microwave data. Multichannel passive microwave imagery has provided near-continuous, daily or bi-daily estimates of sea-ice extent and concentration since late 1978. As such, it represents one of the longest satellite climate records. These time series indicate a significant long-term decline in Arctic sea cover (e.g., Cavalieri & Parkinson 2012). The decline is particularly pronounced during summer, but is seen in all months and in virtually all regions of the Arctic. In the Antarctic, the picture is more complex. Overall there is an increasing trend in pan-Antarctic extent, but with substantial interannual, seasonal and regional variability (Parkinson & Cavalieri 2012); some regions, such as the Bellingshausen and Amundsen seas, have seen a significant decrease in ice cover.

Here we present and verify a new sea-ice concentration product developed at the National Snow and Ice Data Center (NSIDC) under the auspices of the National Oceanic and Atmospheric Administration (NOAA) Climate Data Record (CDR) programme. This new product, hereafter referred to as the sea-ice concentration CDR, is based on well-validated legacy algorithms, but contains several enhancements that meet current CDR requirements for data format, documentation, metadata and processing transparency.

Background on passive microwave sea-ice concentration

Many algorithms have been developed to estimate concentration from passive microwave brightness temperatures (TBs; for summaries and evaluations of several algorithms, see, e.g., Comiso et al. 1997; Partington 2000; Meier 2005; Andersen et al. 2007). The empirically based algorithms differ in their inputs (combinations of different passive microwave frequencies and polarizations) and methodologies, but generally use the same source data: passive microwave TBs from the National Aeronautics and Space Administration (NASA) Nimbus-7 Scanning Multi-channel Microwave Radiometer (SMMR) for 1978–1987 and a series of US Department of Defense Meteorological Satellite Program (DMSP) Special Sensor Microwave Imagers (SSM/I) and Special Sensor Microwave Imager and Sounders (SSMIS) for 1987–present. Gridded SSM/I and SSMIS TBs (Maslanik & Stroeve 2004) are the source for the production of the concentration CDR. The TBs are gridded on a 25-km resolution polar stereographic projection from swath fields obtained from Remote Sensing Systems Inc., in Santa Rosa, CA (Wentz 1997, 2010). While the algorithms yield different absolute sea-ice concentration, area and extent values (e.g., Kattsov et al. 2010), and the magnitude of the differences varies during the annual cycle, they are reasonably consistent through the interannual time series for a given time of year. This means that trend and variability estimates from different algorithms agree well.

Most of the algorithms are well-validated, mature and suitable for tracking trends and variability. Two widely used products are from the NASA Team (NT; Cavalieri et al. 1984) and Bootstrap (BT; Comiso 1986) algorithms. These provide the basis for the CDR and will therefore be discussed in more detail. Both algorithms were developed at NASA's Goddard Space Flight Center (GSFC) and are distributed by the NSIDC (Cavalieri et al. 1996; Comiso 2000). They have been validated through numerous intercomparisons with other passive microwave products as well as co-located visible, infrared and radar imagery

(e.g., Cavalieri et al. 1991; Steffen et al. 1992; Partington 2000; Kwok 2002; Meier 2005; Andersen et al. 2007). Both products include intersensor calibration adjustments to the algorithms and sensor calibrations to assure consistency in extent and concentration estimates across the multiple sensors of the record (Cavalieri et al. 1999; Comiso & Nishio 2008; Cavalieri et al. 2012).

In addition to the basic algorithms and intersensor calibration, a number of quality control steps are applied (Cavalieri et al. 1999; Comiso & Nishio 2008). First, weather filters based on a threshold of TB ratios are used to eliminate low concentration values over open water areas due to wind roughening of the ocean surface or atmospheric moisture. Second, a land-spillover correction is applied to remove spurious ice along coastlines due to mixed ocean–land grid cells; the TB signature from such grid cells is similar to low concentration ice within the algorithms. Third, interpolation is used to fill missing data regions. For isolated missing grid cells, a bilinear interpolation is used to fill missing values in the input TBs. For larger missing regions (often due to missing swaths), a temporal interpolation is done on the resultant concentration fields, filling in the missing values with an average of concentrations from the day before and the day after.

Finally, the fields undergo a manual visual inspection for regions of erroneous concentration data and such data are removed via interactive analysis and replaced with interpolated concentration values. Unfortunately, provenance of these manual corrections is not available, precluding the ability to fully recreate the production of the fields, which is a prerequisite for CDR data sets. Trackable automated methods to replace the manual corrections (such as use of temporal filters) will be investigated for future revisions of the data set.

The NOAA/NSIDC sea-ice concentration CDR

A well-accepted definition of a CDR is a "timeseries of measurements of sufficient length, consistency, and continuity to determine climate variability and change" (NRC 2004: 1). In this sense, the GSFC products are well-suited CDR products. However, the NOAA CDR programme imposes additional criteria in the interest of documentation standards, transparency and reproducibility. These criteria include: (1) self-describing file format (NetCDF4), (2) ISO 19115-2 compliant collection-level metadata, (3) Climate and Forecast (CF) compliant file-level metadata, (4) grid-cell level metadata (data quality fields), (5) fully automated and reproducible processing and (6) open online access to full documentation with version control, including source code and an algorithm theoretical basic

document. The NOAA CDR concentration product presented here has been specifically created to meet these requirements.

The approach to creating the sea-ice concentration CDR is to build upon the legacy of the GSFC algorithm products, enhancing them to meet the NOAA CDR criteria. The CDR was developed by first implementing the NT and BT algorithms at NSIDC. This allows for version control, provenance tracking and full documentation of processing.

To create the CDR concentration parameter, the NT and BT concentration estimates are combined into a single CDR value. This is done by using the BT ice edge (based on a 10% concentration threshold) as the CDR ice edge. Within the ice cover, at each grid cell concentration is estimated from both algorithms and the higher concentration estimate is selected as the CDR concentration value. The rationale for this approach is that passive microwave algorithms tend to underestimate concentration, particularly during the summer melt season with greater underestimation typical in the NT algorithm.

For example, Andersen et al. (2007) found that NT underestimated ice cover by 4.4% in the central Arctic during winter, when passive microwave algorithms are considered most reliable. Agnew & Howell (2003) and Partington et al. (2003) found similar behaviour in comparisons with operational ice charts, which are produced by expert ice analysts combining available imagery. The BT algorithm is dependent, to some extent, on physical temperature and under extreme cold temperatures (such as during winter near the Antarctic coast and in the high Arctic) it tends to slightly underestimate concentration (e.g., Comiso et al. 1997). Concentrations estimated from synthetic aperture radar imagery have been found to generally be near 100% during winter throughout the central Arctic (Kwok 2002), so higher passive microwave values will tend to have lower biases.

During summer, when melt is prevalent, low biases have been found in both algorithms, though generally of larger magnitude in NT (Comiso et al. 1997; Meier 2005). So again, the higher concentration value is likelier to be more accurate. Near the ice edge there is greater ambiguity. The ice edge region is characterized by melt during spring and summer and by thin ice, which has also been found to generally be underestimated (e.g., Cavalieri 1994) during fall and winter. However, due to the low spatial resolution of the passive microwave sensors, the ice edge can be "smeared" out by the algorithms, resulting in detection of ice beyond the true ice edge. Thus, relative performance of the algorithms is quite variable near the ice edge (Meier 2005). Because of

this ambiguity and potential inconsistencies between how the edge is detected by NT and BT, the CDR uses only the BT algorithm (10% concentration threshold) to define the ice edge.

We note that the selection of the higher concentration is somewhat arbitrary and it does not address any existing limitations associated with each algorithm. In fact, such a rule may result in overestimation of concentration in some situations (e.g., Meier 2005). However, as noted in the studies cited above (and several others), the higher concentration will typically be more accurate. Thus, by selecting the higher concentration, the low biases in both NT and BT are ameliorated, and the CDR methodology results in a concentration product with a lower average bias that is based upon two algorithms with a long and well-validated heritage. The CDR product does include as ancillary parameters the original NT and BT concentration for users' convenience; also, the source (NT or BT) for the CDR concentration is noted in a quality assessment flag (see below).

We also note that an enhancement to the NT, commonly referred to as NASA Team 2 (NT2), was developed at the GSFC (Markus & Cavalieri 2000), which ameliorates many of the limitations of the original NT. NT2 compares much more closely to BT, even during melt conditions. However, it uses higher frequency TBs not available on all sensors in the record. It was therefore not chosen as a component for the CDR, although this may be considered in the future if consistency can be assured throughout the record.

The GSFC-produced NT and BT products have a long heritage and have undergone numerous validation studies. Their concentration estimates have been widely disseminated and have been used is numerous studies, including assessments by the Intergovernmental Panel on Climate Change. There is high confidence in the quality of the GSFC products within the scientific community. This was one factor in the selection of the GSFC products for use as the foundation of the NOAA CDR product. Nonetheless, as mentioned above, the GSFC products are lacking in some features that, while they do not affect the quality of concentration retrievals, do not meet NOAA CDR standards. Below, we outline these limitations and how the new concentration product has been designed to meet these standards.

The GSFC-produced NT and BT products contain no grid cell level uncertainty or data quality information, both essential for meeting CDR criteria. Therefore, the CDR product includes two data quality fields. The first is a spatial standard deviation field of both BT and NT concentrations based on a 3 × 3 grid cell neighbourhood for each grid cell. The local spatial standard deviation is

calculated from up to 18 values (nine grid cells each of NT and BT sea-ice concentrations; see figure 3 in Peng et al. [2013] for the schematic diagram) with a minimum of six grid cells with valid values as a threshold for a valid standard deviation. We note that this is not explicitly a quantitative error estimate. However, it serves as an indication of relative data quality between different grid cells. Higher standard deviation values are found when there is larger disagreement between NT and BT concentrations and when there are high spatial gradients in concentration, as illustrated by examples shown in Figs. 1 and 2. Both regimes are indicative of potentially higher uncertainty. Large differences between NT and BT may indicate less confidence in the algorithms and are particularly common to regions where melt occurs. Liquid water or melt ponds on the ice surface contaminates the emission from the ice, reducing the efficacy of the algorithms' ability to calculate concentration. High spatial gradients in concentration occur near the ice edge where sparse and thin ice result in more ambiguous concentrations. It also reflects the low effective resolution of the sensor (ca. 70×45 km for some passive microwave frequencies used in the algorithms), which limits the precision of the ice edge location. The standard deviation parameter (Figs. 1b, 2b) has low values (2–4%) in the interior, where errors are expected to be small and are consistent with concentration errors in cold, consolidated ice conditions found from previous validation studies (e.g., Kwok 2002; Andersen et al. 2007). Near the ice edge, where thin ice and/or melt dominates, the standard deviation parameter has values of 30–40%, which is in range of high errors seen in other validation studies (e.g., Partington et al. 2003; Meier 2005). While not specifically an error estimate, the spatial patterns of this standard deviation field also agree well with other error maps that have been developed for the Enhanced NT2 algorithm (Brucker et al. 2014) and the European Ocean and Sea Ice Application Satellite Application Facility product (Eastwood et al. 2011).

Thus, the standard deviation field provides a quantitative indication of relative uncertainty. A second quality assessment field contains flags that note salient conditions for each grid cell, including melt state, proximity to coast (indicating potential land-spillover contamination not removed by the automated filter) and low concentration grid cells (which typically have higher errors). These two fields allow users to assess the quality of each CDR concentration estimate. While a quantitative error estimate is desirable, it is difficult for sea ice because of the spatial and temporal sampling difference between the passive microwave data and available validation data, as well as uncertainties in the validation sources themselves (e.g., other satellite imagery). As noted above, the quality assessment field also denotes which algorithm's concentration was used in the CDR parameter for a given grid cell.

Another issue with the GSFC products is that manual quality control is used in their production. It is clear that the automated processing results in some spurious results and that manual quality control by expert scientists knowledgeable about the algorithms and concentration fields result in improved fields. However, as beneficial as the manual corrections may be, such an approach violates the CDR requirement for full transparency and reproducibility. Therefore for the CDR concentration, all processing is fully automated and the source code is made available through the NOAA CDR programme.

Finally, while the GSFC NT and BT fields have little or no file-level metadata and are distributed in a flat-binary format, the CDR is produced in the self-describing NetCDF4 format with fully compliant CF metadata. Such metadata and self-describing file formats are becoming more and more important as the data are being used by a broader community (i.e., beyond sea-ice experts) and provenance and future accessibility are becoming more of a focus in the international community.

Version 1 of the sea ice concentration CDR was initially produced for the SSM/I period, 1987–2007 and it is this version that is evaluated here. It has since been reprocessed to Version 2 and will be updated quarterly in the future. Version 2 updates the time series through 2012 using SSMIS, along with minor changes to metadata and the format of data quality fields. No changes were made to the CDR concentration processing. The verification presented here is therefore equally valid for Version 1 and Version 2. In addition to the concentration CDR and associated data quality fields, the GSFC BT and NT fields are included along with a combined concentration estimate that is produced from the GSFC concentrations using the same method to produce the CDR concentration (Table 1). This combined GSFC parameter is the main point of comparison for the CDR estimates in this paper and is hereafter referred to simply as "GSFC." Another feature of the GSFC parameter is that it extends the sea ice record through the SMMR period. For the initial version of the CDR, the SMMR period is not included due lack of provenance in the initial processing of SMMR by GSFC and concerns over data quality that in the initial processing required significant manual correction (Parkinson, pers. comm.). We plan to investigate extending the processing of the CDR concentration parameter for the SMMR period in the future.

Specifics of the CDR product and processing methods are provided in a companion paper (Peng et al. 2013).
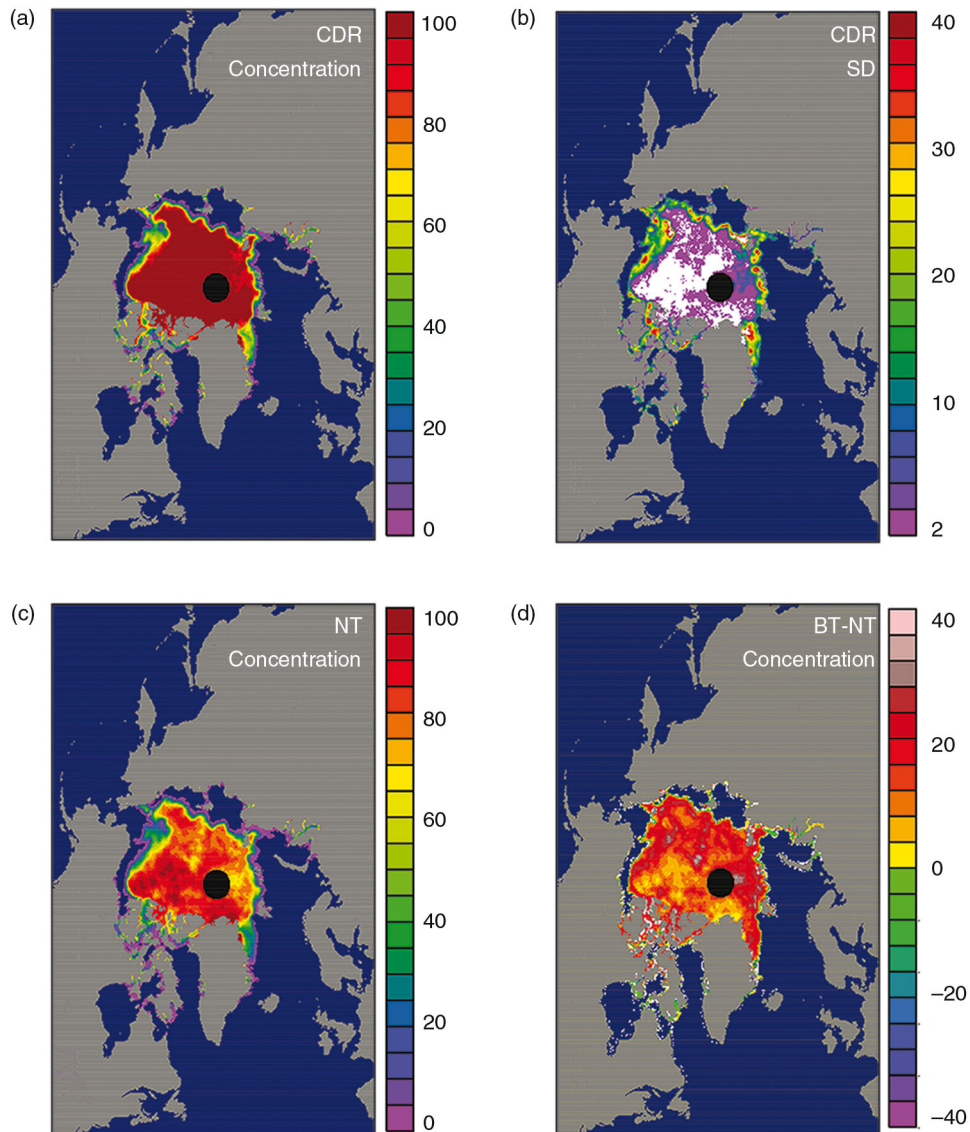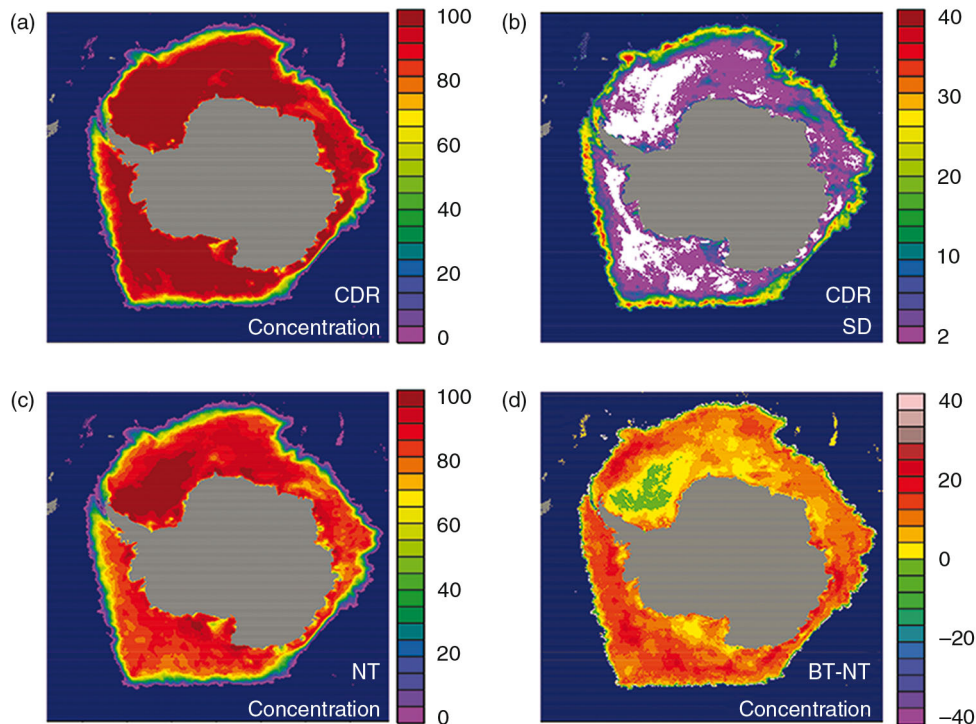
Fig. 1 Spatial distribution of: (a) monthly Climate Data Record (CDR) concentrations, (b) local standard deviation (SD), (c) monthly NASA Team (NT) concentrations and, (d) concentration difference between monthly Bootstrap (BT) and NT estimates for the Northern Hemisphere in September 2000. The units are percent concentration.

The data are available from the NSIDC (http://nsidc.org/ g02202.html) along with accompanying documentation and an Algorithm Theoretical Basis Document (Meier 2012). The ATBD also includes further details of the NT and BT algorithms and discussion of data quality and error sources.

Verification of the CDR

The algorithms included in the sea ice concentration CDR have been widely validated in numerous studies (e.g., Cavalieri et al. 1991; Steffen et al. 1992; Comiso et al. 1997; Partington 2000; Kwok 2002; Meier 2005; Andersen et al.

2007). Here we verify the CDR estimates via comparison with the combined GSFC estimates created from the original NT and BT algorithm products (in the same manner as the CDR concentration, that is, the highest value of NT and BT). As noted above, the primary differences in the CDR and the GSFC products are: (1) missing grid cells are not filled with interpolation, (2) no manual quality control is performed and (3) processing is done at NSIDC (Table 1). A final difference is that NSIDC uses the most recent version of the input TBs available at the time of initial processing (Remote Sensing Systems versions 4 or 6) while GSFC has not reprocessed the NT product with newer TB versions (BT has been reprocessed). The input data therefore have

Fig. 2 Spatial distribution of: (a) monthly Climate Data Record (CDR) concentrations, (b) local standard deviation (SD), (c) monthly NASA Team (NT) concentrations and, (d) concentration difference between monthly Bootstrap (BT) and NT for the Southern Hemisphere in September 2000. The units are percent concentration.

some differences for part of the period. However, these TB version differences are generally quite small.

We assess here the effect of these differences on estimates of concentration, area and extent. "Concentration" here is defined as the percent coverage of a grid cell or region. "Area" is the total surface area of sea ice, summed from the concentration-weighted area of each grid cell. "Extent" is the total surface covered by ice of at least 15% (i.e., not weighted by concentration, just summing the area of all grid cells with $\geq 15\%$ ice).
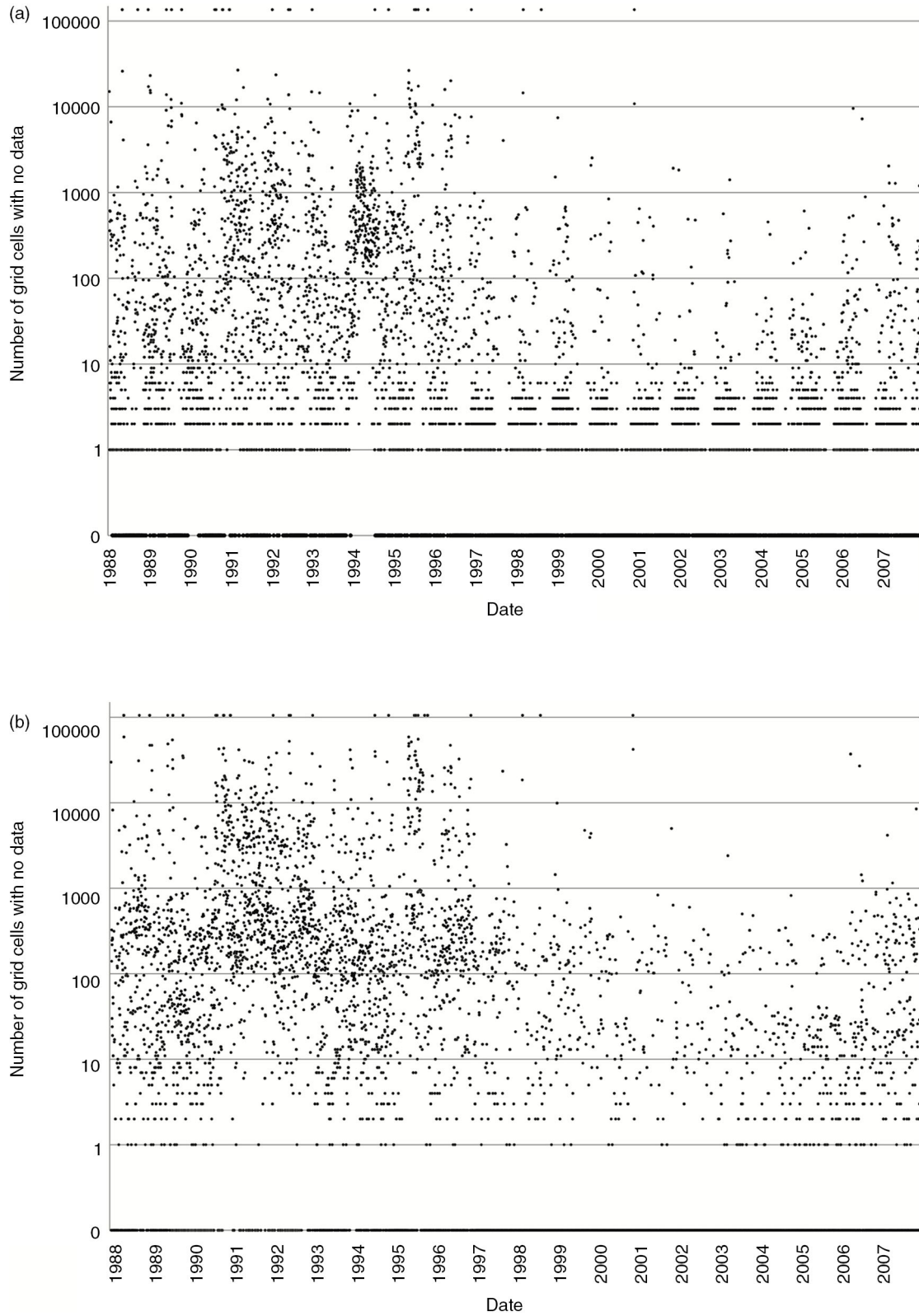
Missing grid cells

First, we analyse the number of missing grid cells in the CDR field because this represents the most noticeable difference with the GSFC fields. Missing grid cells are only flagged in regions of "possible ice," that is, non-land areas that are not filtered by the ocean masks (see Meier 2012 for more details). Essentially, missing cells are counted for sea-ice-covered areas and a surrounding buffer of open ocean. Overall, most days have few (≤ 10)

Table 1 Summary of the characteristics of the National Oceanic and Atmospheric Administration Climate Data Record (CDR) concentration and the comparison combined Goddard Space Flight Center (GSFC) concentration. Main differences between the two are shown in boldface.

Description	CDR	GSFC
Source TBs[a]	RSS[b]-based polar stereo gridded	RSS-based polar stereo gridded
RSS TB version	**Ver. 4, ver. 6**	**Ver. 2, ver. 4**
Algorithms	NT, BT[c]	NT, BT
Algorithm processing location	**NSIDC[d]**	**GSFC**
Ice edge definition	BT $\geq 10\%$	BT $\geq 10\%$
Concentration value	Greater of NT, BT	Greater of NT, BT
Automated weather, coast filters	Yes	Yes
Interpolation to fill missing data?	**No**	**Yes**
Manual quality control	**No**	**Yes**
Period of data	**July 1987–December 2007**	**October 1978–December 2007**

[a]Brightness temperatures. [b]Remote Sensing Systems Inc. [c]NASA Team, Bootstrap. [d]National Snow and Ice Data Center.

Fig. 3 Number of missing grid cells over the full grid (136 192 grid cells total) for each day, 2 January 1988–31 December 2007 in (a) the Northern Hemisphere and (b) the Southern Hemisphere. The y axis is logarithmic. Values >100 000 represent days with no data (i.e., all grid cells are missing).

Table 2 Number of days over 1 January 1988–31 December 2007 in each hemisphere with missing grid cells in each range. There were no days with >40000 missing grid cells other than days with no data.

No. of missing grid cells	Northern Hemisphere	Southern Hemisphere
0	2615	3936
1–10	2693	551
11–100	865	854
101–1000	747	1370
1001–10000	292	402
10001–20000	31	65
20001–30000	6	28
30001–40000	0	25
No data	45	45

or no missing data (Fig. 3, Table 2). Days with few missing grid cells are generally complete files (i.e., no missing swaths of input TBs), with scattered grid cells of no data resulting from the gridding of the input passive microwave TBs. These occur because the gridded TBs are under-sampled relative to the sensor footprint and some grid cells do not contain the centre of any TB footprint. These footprint-induced missing grid cells happen more frequently nearer the equator (where there is less overlap between swaths) and therefore tend to most affect Northern Hemisphere ice cover during the winter (when

the ice edge can extend to ca. 45° N latitude). Higher numbers of missing grid cells (on the order of 100–10000) result from missing swaths of data, due primarily to satellite operations or recording failures at the time of data collection. In the Northern Hemisphere, there is a noticeable cluster of missing data during 1994 when there are considerable missing data. In the Southern Hemisphere, there are generally more days in the 100–10000 grid cells range. This is largely due to the more conservative ocean masks used there for both algorithms that allow a large region of "possible ice" compared to the north (again see Meier 2012 for more details). This larger region allows larger chunks of missing data from swath dropouts.

Overall there are relatively few days with substantial amounts of missing grid cells, so the missing data results in a relatively small difference with the GSFC fields that interpolate to fill in the missing cells. The CDR did not use interpolation to keep processing more straightforward and transparent and to allow users to use their own discretion on how to deal with missing data. Interpolation is being considered for future versions, depending on user feedback, but if implemented all processing steps will be fully documented and interpolated grid cells will
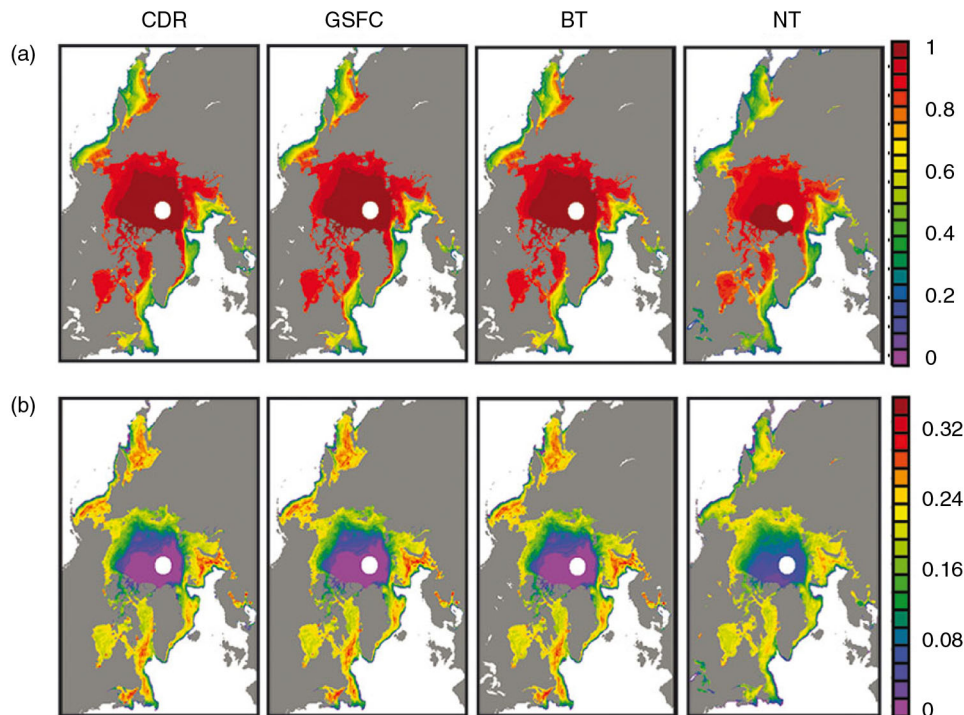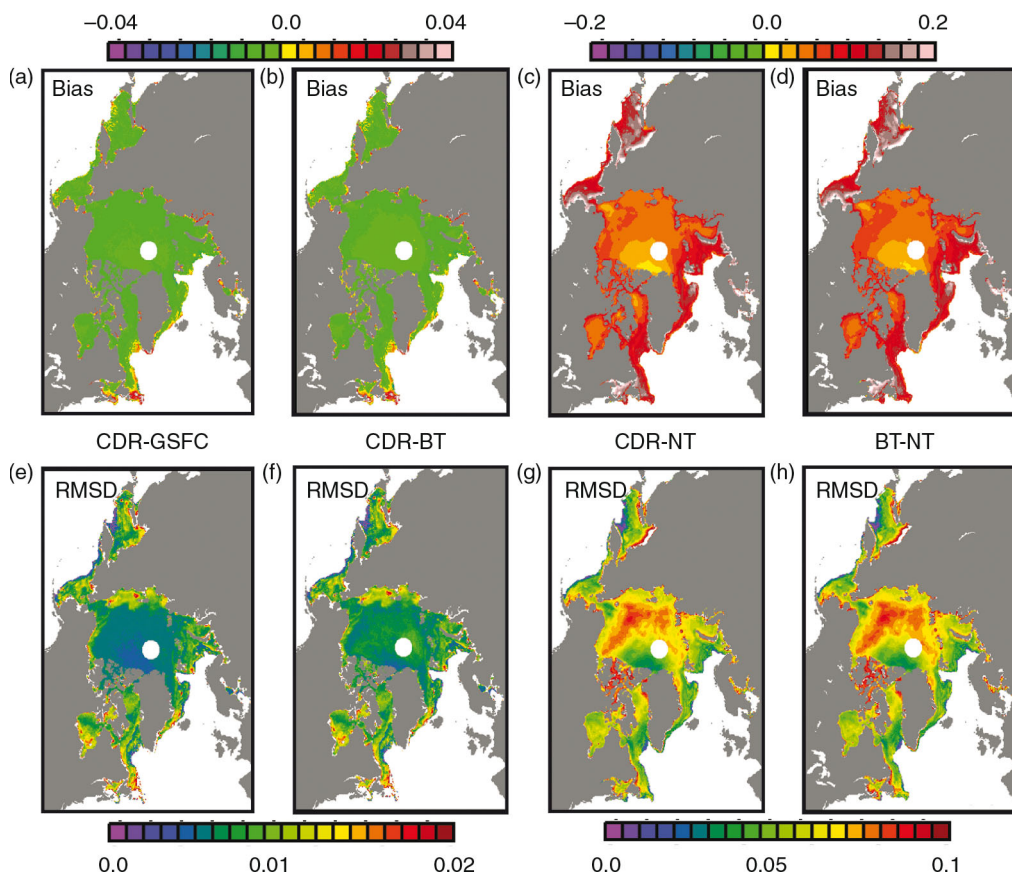

Fig. 4 Spatial distribution of 20 years (1988–2007) (a) mean and (b) standard deviation (SD) of monthly sea-ice concentrations from the National Oceanic and Atmospheric Administration Climate Data Record (CDR), Goddard Space Flight Center (GSFC), Bootstrap (BT) and NASA Team (NT) algorithms in the Northern Hemisphere. Units are fraction ice concentration (0–1). Grid cells with sea-ice concentrations less than 0.15 (15%) are not included in the calculations.
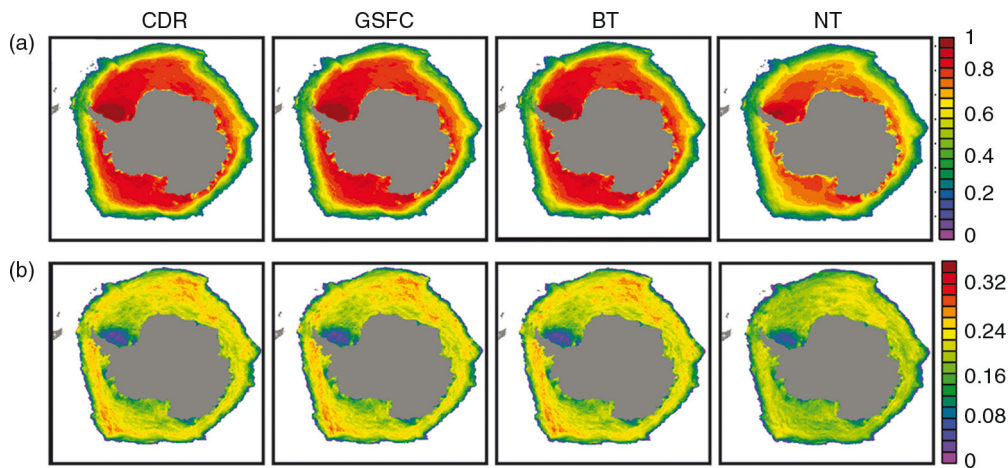
Fig. 5 Spatial distribution of 20 years (1988–2007) (a) mean and (b) standard deviation (SD) of monthly sea-ice concentration from the National Oceanic and Atmospheric Administration Climate Data Record (CDR), Goddard Space Flight Center (GSFC), Bootstrap (BT) and NASA Team (NT) algorithms in the Southern Hemisphere. Units are fraction ice concentration (0–1). Grid cells with sea ice concentrations less than 0.15 (15%) are not included in the calculations.

Fig. 6 Spatial distribution of bias (mean difference) and root mean square difference (RMSD) of monthly sea ice concentration anomaly between: (a), (e) the National Oceanic and Atmospheric Administration Climate Data Record (CDR) and Goddard Space Flight Center (GSFC); (b), (f) CDR and Bootstrap (BT); (c), (g) CDR and NASA Team (NT); and (d) and (h) BT and NT in the Northern Hemisphere. Note that the scale factor for (c), (d), (g) and (h) is five times larger than that of (a), (b), (e) and (f). Units are in fraction concentration (0–1). Grid cells with sea-ice concentrations less than 0.15 (15%) are not included in the calculations.

be flagged. For consistency in the following comparisons, missing cells are not included in total area and extent calculations.

Global spatial distribution of means, standard deviations, mean difference and root mean square difference

Before we show the results of monthly extent and area comparison, it is beneficial to provide the global spatial distributions of CDR and GSFC fields, including a merged GSFC that combines the GSFC-processed NT and BT estimates in the same manner as the CDR to produce a GSFC-based pseudo-CDR concentration field. Figures 4 and 5 display the mean and standard deviation of 20 years of monthly CDR sea-ice concentration fields (January 1988–December 2007) in the Northern and Southern Hemisphere, respectively. The figures show the very similar spatial distributions of means and standard deviation for CDR, GSFC and BT, while NT displays somewhat different spatial distributions. Figures 6 and 7 show the mean difference (bias relative the reference product) and root mean square difference (RMSD) referenced to GSFC, BT and NT. The mean difference and RMSD of BT and NT concentrations are also shown. The CDR and GSFC fields are virtually indistinguishable from each other, with near-zero bias and RMSD values <2%. The CDR and BT fields are also quite similar. There are larger differences between the

CDR and NT concentration fields, particularly in the Arctic seasonal ice zone, where summer melt effects are large during summer and throughout the Antarctic. This is not unexpected because of the NT's known low biases in these regions (e.g., Comiso et al. 1997). These results demonstrate that there is strong consistency between GSFC processing and the NSIDC CDR processing and show the differences between the CDR and the constituent NT and BT concentration.

Monthly extent and area comparison

The differences in processing between the GSFC fields and NSIDC-processed CDR fields are minimal (outside of the missing grid cells). The CDR time series of monthly total extent and area exhibit only small differences with estimates from the GSFC fields. In the Northern Hemisphere, CDR generally has a higher extent, with the high bias peaking during summer (Fig. 8a) where CDR is up to 400 000 km^2 higher in some years. This is due to remaining false coastal ice that the land-spillover correction does not remove. These grid cells have presumably been removed manually by GSFC, but are not in the automated CDR processing. In the future, we plan to investigate automated methods that can substitute for the manual corrections. The overestimate by CDR due to this effect peaks during summer because of a larger perimeter of ice-free coast as well as the effect of the warmer land surface temperatures. The only significant
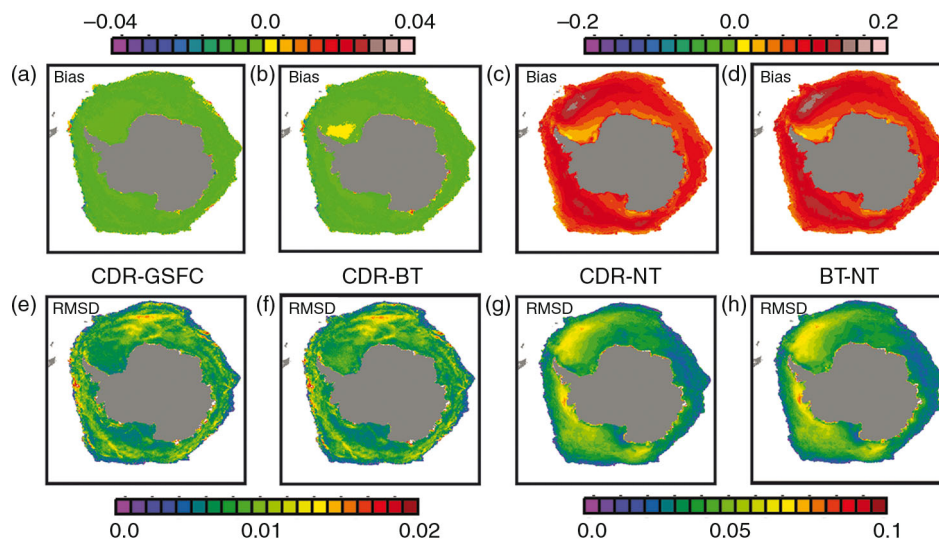
Fig. 7 Spatial distribution of bias (mean difference) and root mean square difference (RMSD) of monthly sea ice concentration anomaly between: (a), (e) the National Oceanic and Atmospheric Administration Climate Data Record (CDR) and Goddard Space Flight Center (GSFC); (b), (f) CDR and Bootstrap (BT); (c), (g) CDR and NASA Team (NT); and (d) and (h) BT and NT in the Southern Hemisphere. Note that the scale factor for (c), (d), (g) and (h) is five times larger than that of (a), (b), (e) and (f). Units are in fraction concentration (0–1). Grid cells with sea-ice concentrations less than 0.15 (15%) are not included in the calculations.
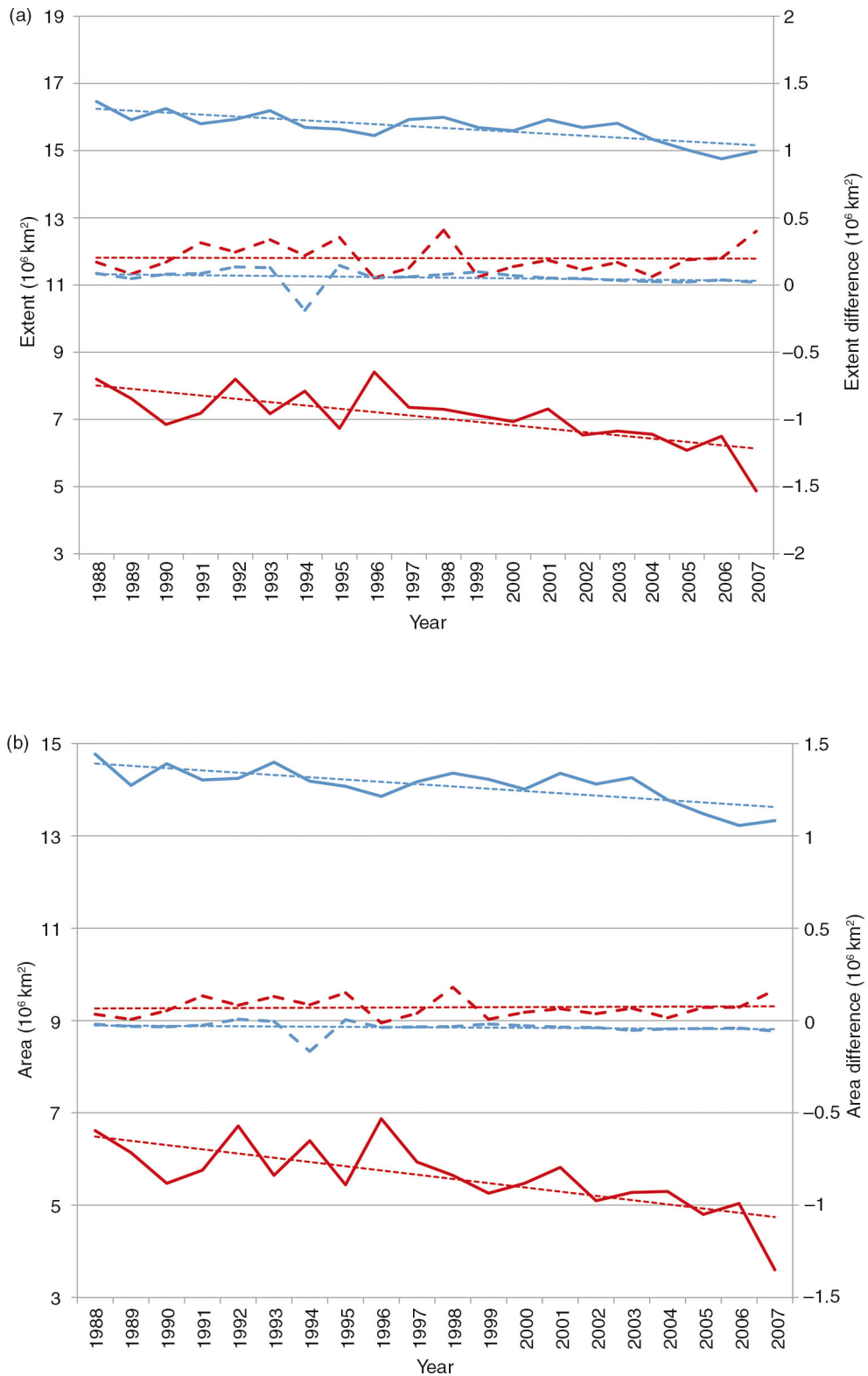
Fig. 8 Time series of monthly Northern Hemisphere the National Oceanic and Atmospheric Administration Climate Data Record (CDR) (a) extent and (b) area for 1988–2007 (thick solid lines: blue for March and red for September) and difference between CDR and Goddard Space Flight Center estimates (dashed lines). Note the different y axis scales for the extent/area (left axis) and the differences (right axis). The dotted lines are linear trends.
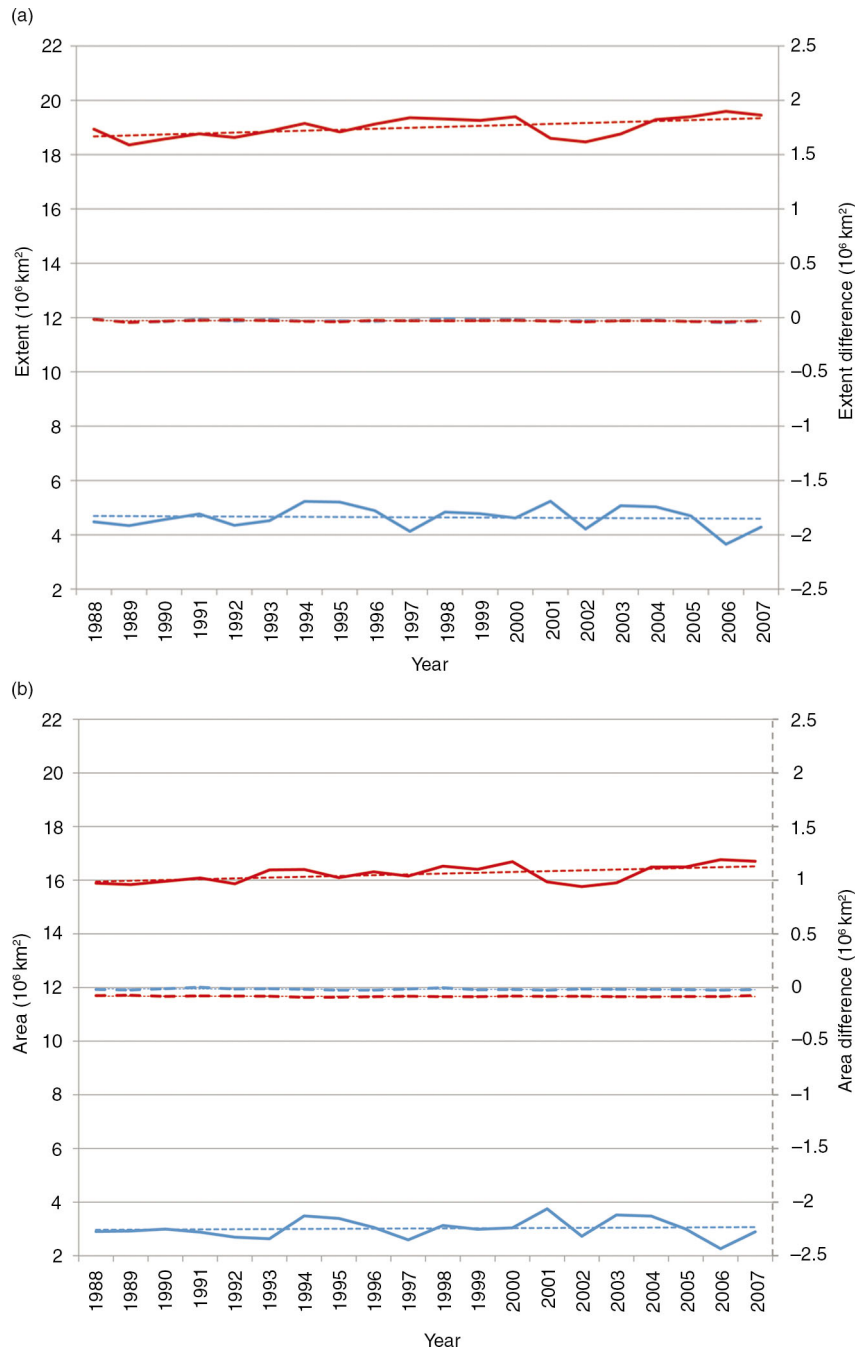
Fig. 9 Times series of monthly Southern Hemisphere National Oceanic and Atmospheric Administration Climate Data Record (CDR) (a) extent and (b) area for 1988–2007 (thick solid lines: blue for March and red for September) and difference between CDR and Goddard Space Flight Center estimates (dashed lines). Note the different y axis scales for the extent/area (left axis) and the differences (right axis). The dotted lines are linear trends.

period of extent underestimation by the CDR is during early 1994; this is due to a substantial amount of missing data during the period, which skews the monthly estimates lower in the CDR compared to GSFC.

The Northern Hemisphere area estimates show a much smaller difference and near-zero bias (Fig. 8b). This is because the false coastal ice is generally low concentration (but >15%) and therefore has a much smaller effect on area than on extent. The largest overestimation is only 180 000 km^2 in September 1998 and most differences are 50 000 km^2 or less. The effect of the 1994 missing data is also apparent in the area comparison.
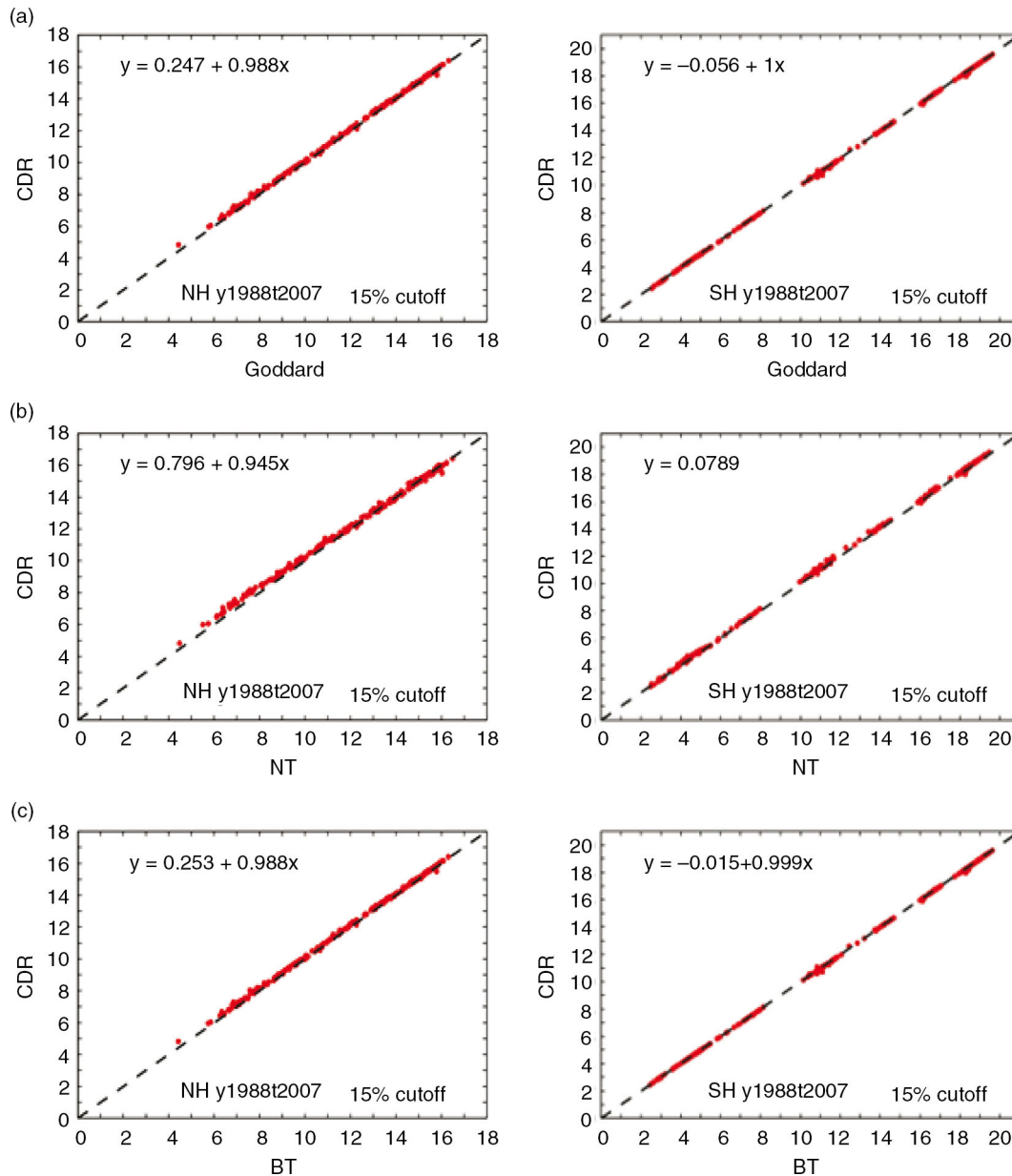
Fig. 10 The scatter diagram of monthly sea ice extents (10^6 km^2) from monthly National Oceanic and Atmospheric Administration Climate Data Record (CDR) and (a) Goddard Space Flight Center, (b) NASA Team (NT) and (c) Bootstrap (BT) data. The left column of diagrams is for the Northern and the right is for the Southern Hemisphere.

In the Southern Hemisphere, the extent difference between CDR and GSFC is smaller than in the Northern Hemisphere (Fig. 9a), mostly below 50000 km^2. This is because there is minimal impact of the land-spillover effect since so little of the Antarctic coast is ice-free (essentially none during winter and most of spring and fall) and the land is mostly covered with glacial ice and remains cold through the summer. To the degree that there is a bias, the CDR slightly underestimates extent compared to GSFC, with a slightly more pronounced

effect during the summer minimum, when the difference approaches 100000 km^2 in some years. This is when concentrations are low and many grid cells are near the 15% threshold, making the extent sensitive to small processing differences (e.g., the Remote Sensing Systems TB version).

Southern Hemisphere area also shows a slightly negative bias for CDR, but with an opposite seasonal cycle from the extent (Fig. 9b). The small summer bias in area compared to the larger winter extent bias again

Table 3 Confusion matrix for comparison of National Oceanic and Atmospheric Administration Climate Data Record (CDR) and Goddard Space Flight Center (GSFC) sea-ice extent. a and d represent correct "forecasts" counts for a given time period, while b and c are incorrect, using GSFC as the "correct" estimate.

Class type	GSFC sea ice	GSFC no-ice
CDR sea ice	a	b
	Correct ice	False ice
CDR no-ice	c	d
	False no-ice	Correct no-ice

indicates low concentration ice near the 15% threshold. The more pronounced low bias during the winter likely reflects the small processing differences influencing a much longer ice edge as the sea ice encircles the entire continent.

A scatter diagram (Fig. 10) of monthly CDR and GSFC extents further demonstrates the close agreement between the two. The relationship between the two is predominantly linear, with little scatter. A slight positive bias of the CDR relative to GSFC is seen in the Northern Hemisphere, due (as mentioned above) primarily to false ice from land-spillover errors. Similar results can be seen from the scatter diagram of monthly CDR and BT (Fig. 10) while a more noticeable positive bias of the CDR relative to NT can be seen in both hemispheres, more so for the Northern Hemisphere (Fig. 10).

Confusion matrix

Another way to assess the differences in the CDR and GSFC is via a "confusion matrix" that compares binary conditions (in this case, "ice" vs. "no-ice") from two different estimates (CDR and GSFC). Such an approach is often used to assess the quality of weather forecasts (Murphy & Winkler 1987; Wilks 2011) and has been used to assess model predictions of sea-ice extent with observations (Van Woert et al. 2003). Here we use the

approach to assess the CDR quality compared to GSFC, with GSFC used as the reference (i.e., "truth") because it is based on the best-validated products and includes manual corrections. Thus, this is a measure of how well the CDR processing replicates the validated GSFC processing and assesses the effect of the CDR-imposed limitations on the processing (i.e., no manual correction). Table 3 shows the confusion matrix conventions for the evaluation between the CDR and GSFC estimates.

An "ice" event is categorized as a grid cell whose area is covered by at least 15% sea ice (as estimated by the algorithm) while a "no-ice" event means a grid cell is covered with less than 15% sea ice. A "correct" ice or no-ice occurrence corresponds to when both CDR and GSFC have ice or no-ice at the same cell, respectively. An "incorrect" ice classification occurs when CDR indicates an ice grid cell while GSFC indicates no-ice for that cell; an incorrect no-ice classification indicates that CDR shows no-ice while GSFC shows ice in the same grid cell. The event counts are carried out here for March and September using daily data for a period of 20 years (1988–2007).

The summary of analysis of the confusion matrix for the CDR and GSFC (Table 4) shows similar results as indicated in the time series comparison. There is the expected contrast between correct ice and correct no-ice between March and September due to the seasonal cycle in each hemisphere. However, combining these two "correct" results make up the large majority of the cases. There is a notable percentage of false ice in the Northern Hemisphere due to the land-spillover issue, with a higher percentage during September than in March. Overall, incorrect CDR designations of ice or no-ice make up at most ca. 1% of the grid cells. Other months exhibit similar results.

As it is not practical to show monthly confusion matrices for all 20 years, a confusion matrix diagram (Fig. 11) is developed (following Taylor 2001) to display not only the percentage occurrence of four events as shown in Table 3 but also their temporal evolution.

Table 4 A summary of results of confusion matrix for September and March for the Northern (NH) and Southern (SH) hemispheres for the 20-year period from 1988 to 2007. The mean, minimum and maximum percentages for each month are provided as well as the overall range of percentages.

Class Mon/HH	a (%) Correct CDR ice[a]			b (%) False CDR ice[b]			c (%) False CDR no-ice[c]			d (%) Correct CDR no-ice[d]		
	Mean	Min	Max	Mean	Min	Max	Mean	Min	Max	Mean	Min	Max
Mar/NH	36.2	33.9	38.0	0.27	0.14	0.47	0.007	0.002	0.015	63.5	61.7	65.9
Sep/NH	14.5	9.23	17.8	0.57	0.18	1.13	0.003	0.000	0.015	84.9	82.1	89.8
Mar/SH	7.97	6.34	9.25	0.02	0.009	0.04	0.000	0.000	0.002	92.0	90.7	93.6
Sep/SH	37.2	35.9	38.4	0.014	0.006	0.05	0.002	0.000	0.004	62.8	61.6	64.1
Range	6.34–38.4			0.006–1.13			0.00–0.015			61.6–93.6		

[a, b, c, d]The states of the confusion matrix, as provided in Table 3.
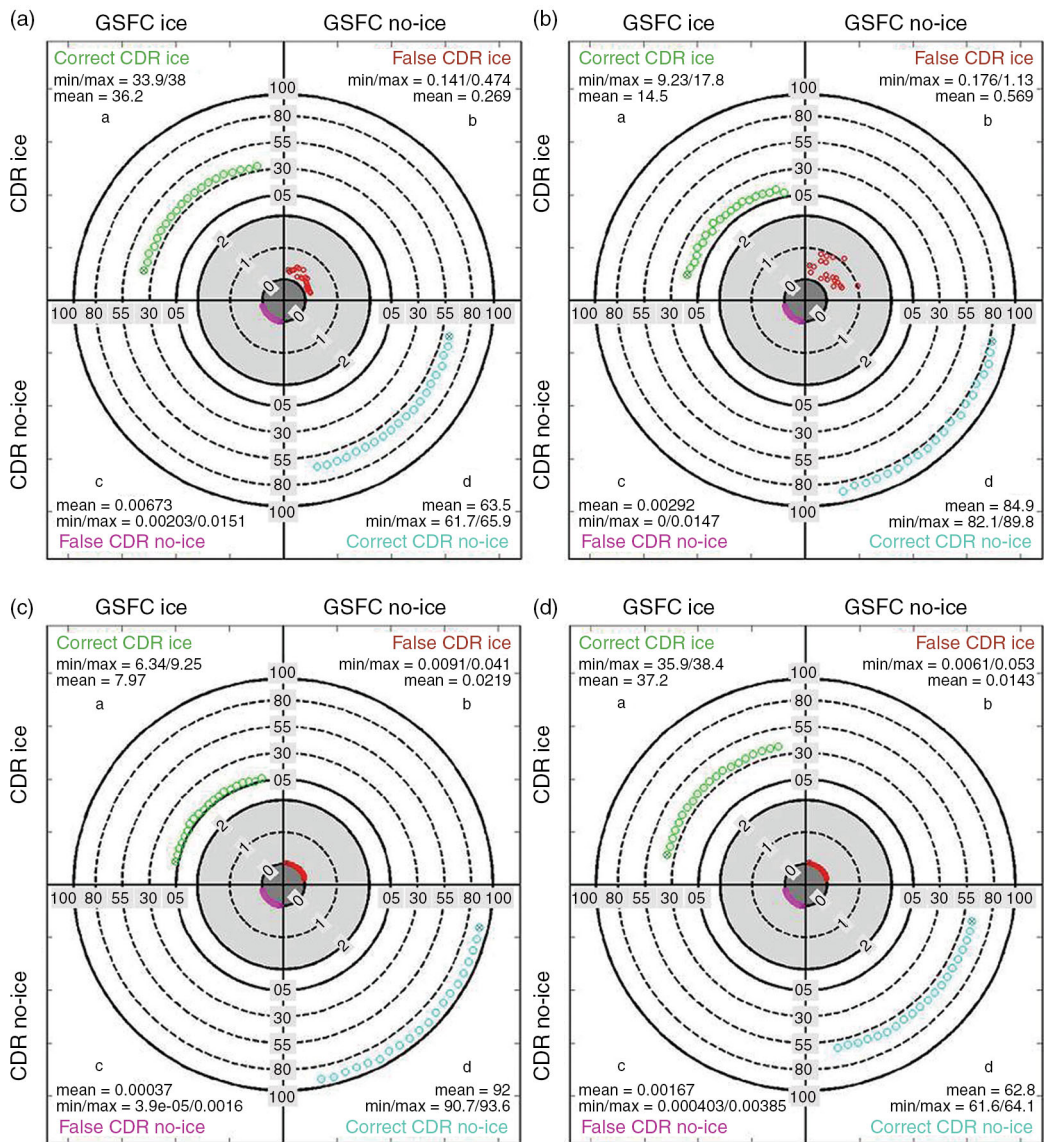
Fig. 11 Confusion matrix diagrams for the (a) and (b) Northern Hemisphere and (c) and (d) Southern Hemisphere in (a) and (c) March and (b) and (d) September. GSFC refers to the sea ice fields produced by Goddard; CDR are the climate data record fields. Note that different scales are used in the shaded areas. The circled ''x'' marks the value of the percentage occurrence of year 1988 for the event, with adjacent empty circles moving clockwise representing subsequent years through 2007.

The performance of the CDR compared to GSFC is consistent through the 20 years of the time series, with little change in the percentages over time, as seen in the confusion matrix diagram. The only significantly non-zero incorrect results are in the upper left quadrant of the Northern Hemisphere representing "false ice" due to the land-spillover effect.

How well the CDR ice or no-ice event estimates perform against the GSFC ice or no-ice event estimates, that is, "truth" or the reference, is normally measured quantitatively in term of correct ice and no-ice occurrences proportionally to the total event counts, that is, accuracy, which is defined as follows:

$$\text{Accuracy}\,(\%) = (a + d)/(a + b + c + d) \times 100$$

The accuracy for both hemispheres is quite high (Figs. 12a, b, 13a, b), more so for the Southern Hemisphere as the percentage of no-ice occurrences tends to dominate the results (Figs. 11, 13a, b).
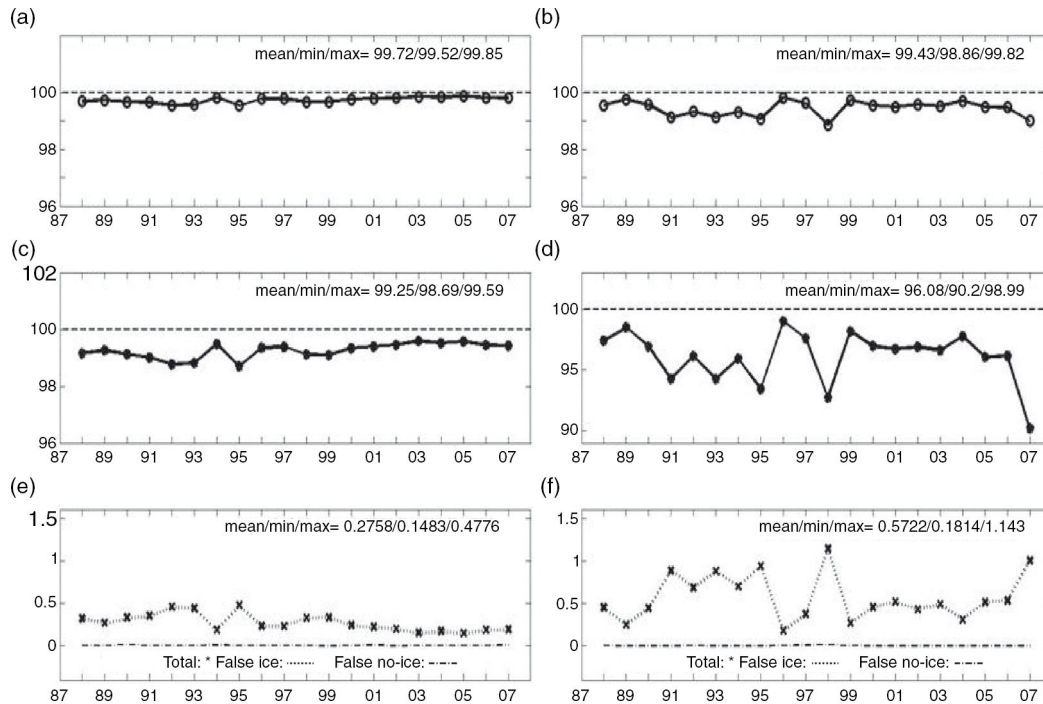
Fig. 12 Temporal evolution of (a) and (b) accuracy, (c) and (d) precision, (e) and (f) false/incorrect classification of the National Oceanic and Atmospheric Administration Climate Data Record (CDR parameter in (a), (c) and (e) March and (b), (d) and (f) September for the Northern Hemisphere for the period of years 1988–2007. A 15% concentration cut-off is used to delineate ice and no-ice classification and missing grid cells are not included. The mean, minimum and maximum monthly values over the entire 1988–2007 period are given at the top of each plot.

Since how well the CDR estimates an ice event correctly is more critical and its occurrences are substantially less frequent than the no-ice occurrences, an alternative parameter, precision, is a more useful indicator of skill. Precision, sometimes referred to as threat score or critical success index, is defined as the percentage of correct ice occurrences over the total number of ice event occurrences including false ice and no-ice counts and is computed as:

$$\text{Precision (\%)} = a/(a + b + c) \times 100$$

Precision (Figs. 12c, d, 13c, d) tends to be slightly lower than accuracy with slightly lower values in late melting seasons that are consistent with false ice (Figs. 12e, f, 13e, f) but shows the variation better. One distinct feature is the lower precision with higher false ice percentage in September 2007 in the Northern Hemisphere (Fig. 12d, f), when the previous Arctic ice minimum occurred. This larger discrepancy is likely related to the extreme low extent (a record at the time) and the large amount of open water present during September 2007. This resulted in a relatively large number of false ice grid cells in the CDR due to open coastlines around much of the perimeter of the Arctic Ocean.

Comparison of trends

One of the important applications of a climate record is to track trends. The CDR yields trends over the 1988–2007 period that are not significantly different than the trends from the GSFC trends (Table 5; Figs. 8, 9). The trend differences between CDR and GSFC are small compared to the absolute trend in all months in both hemispheres, with the difference trend lines nearly horizontal (Figs. 8, 9). Also, the differences are much smaller than the difference standard deviation, indicating that the differences are not statistically significant. The CDR product therefore captures the same trends as the GSFC estimate and is reliable for hemispheric trend analysis.

Trends from the NT and BT algorithm products have been widely disseminated (recently, e.g., Comiso & Nishio 2008; Cavalieri & Parkinson 2012), including use in the Intergovernmental Panel on Climate Change assessment reports. To insure that the CDR trends are consistent with the individual algorithm trends from GSFC, we also compare extent and area trends between the CDR and BT and NT. The NT algorithm yields much lower total areas overall (Figs. 14, 15) than the BT and CDR estimates, which are very close to each other. However, the trends and interannual variability are consistent between all
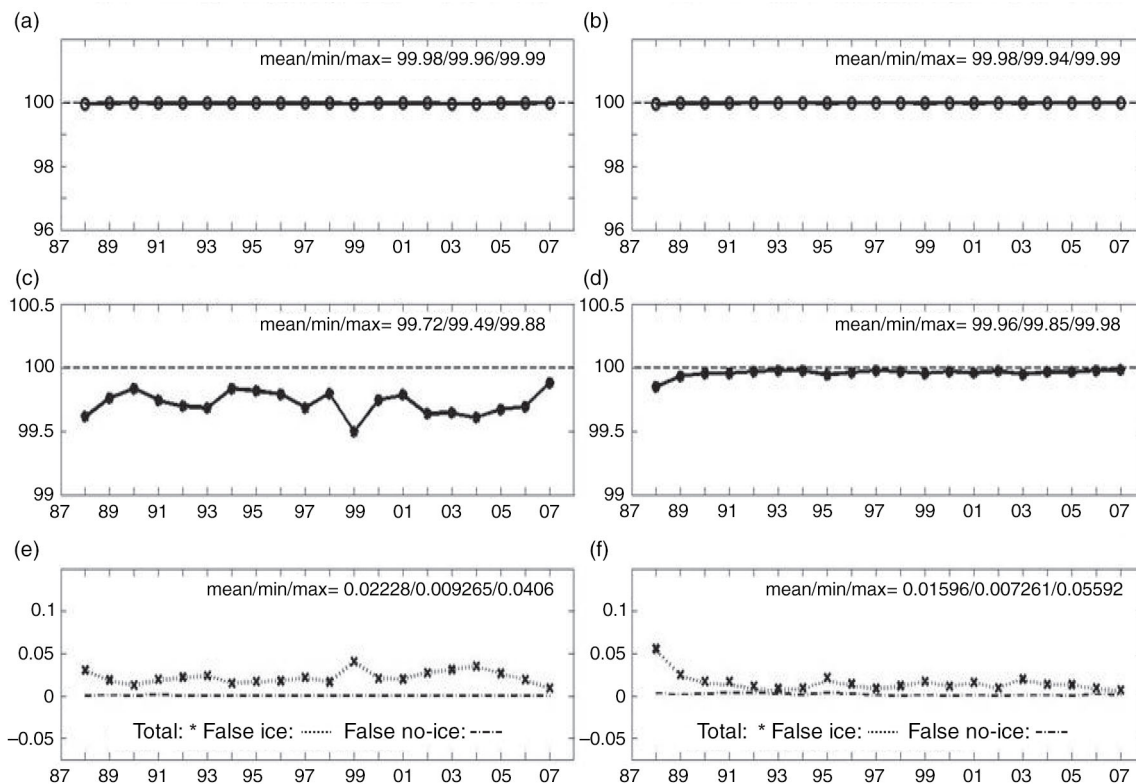
Fig. 13 Temporal evolution of (a) and (b) accuracy, (c) and (d) precision, (e) and (f) false/incorrect classification of the National Oceanic and Atmospheric Administration Climate Data Record (CDR) parameter in (a), (c) and (e) March and (b), (d) and (f) September for the Southern Hemisphere for the period of years 1988–2007. A 15% concentration cut-off is used to delineate ice and no-ice classification and missing grid cells are not included. The mean, minimum and maximum monthly values over the entire 1988–2007 period are given at the top of each plot.

three products, with only small, statistically insignificant differences between them (Tables 6, 7). Extent trend values (not shown) are similar. The CDR can therefore provide trend estimates with similar confidence as the GSFC heritage algorithms.

Summary

This paper presents a new passive microwave sea ice concentration product developed under the guidance of the NOAA CDR programme. Several passive microwave

Table 5 Monthly sea-ice extent trend estimates (in km^2) over 1988–2007 for the National Oceanic and Atmospheric Administration Climate Data Record (CDR) and the difference between CDR and Goddard Space Flight Center (GSFC) for the Northern and Southern Hemispheres.

Month	Northern Hemisphere		Southern Hemisphere	
	CDR trend	CDR–GSFC trend (SD)	CDR trend	CDR–GSFC trend (SD)
January	−63 500	−2100 (49 000)	−5300	−200 (20 400)
February	−55 300	−1700 (98 700)	+13 500	+500 (14 200)
March	−57 100	−2600 (68 300)	−5400	−300 (9900)
April	−52 000	−1300 (48 500)	+4100	+900 (16 800)
May	−28 700	−1500 (53 100)	+2400	−1800 (40 500)
June	−37 400	−3700 (87 900)	+17 700	−1200 (21 900)
July	−76 500	−3800 (67 400)	+22 500	+300 (8000)
August	−82 200	−5700 (102 500)	+11 600	+1300 (48 400)
September	−98 700	−400 (111 300)	+35 400	−300 (6600)
October	−78 800	+2700 (39 300)	+29 900	+3000 (68 200)
November	−83 400	+1600 (46 800)	+18 000	+1300 (49 600)
December	−57 200	+4200 (63 700)	+8500	−5700 (121 800)

(a)

(b)
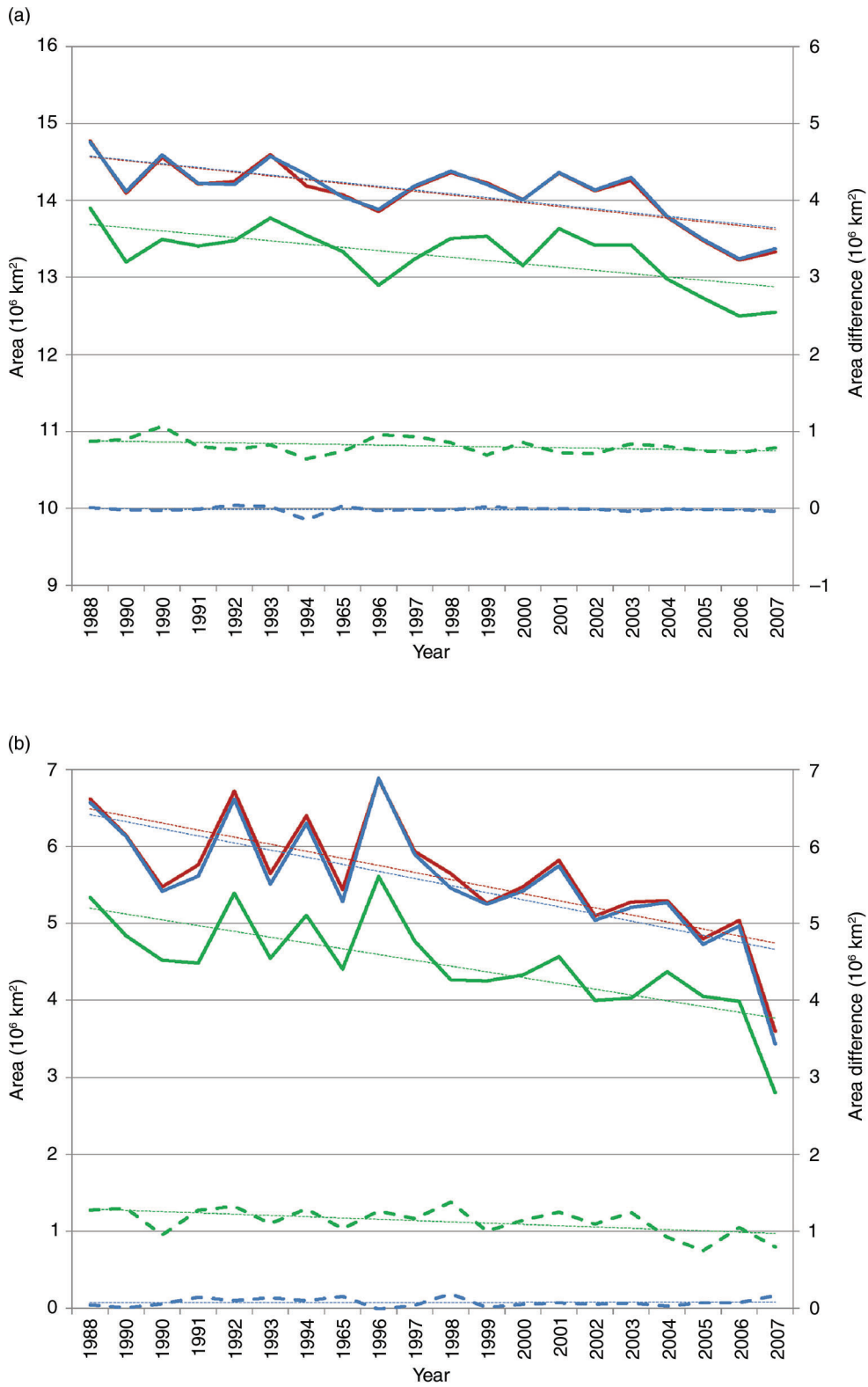
Fig. 14 Northern Hemisphere CDR ice area for (a) March and (b) September from the National Oceanic and Atmospheric Administration Climate Data Record (CDR; red), Bootstrap (blue) and NASA Team (green), in solid lines. Dashed lines are the difference between CDR and Goddard Space Flight Center. Dotted lines are linear trends.
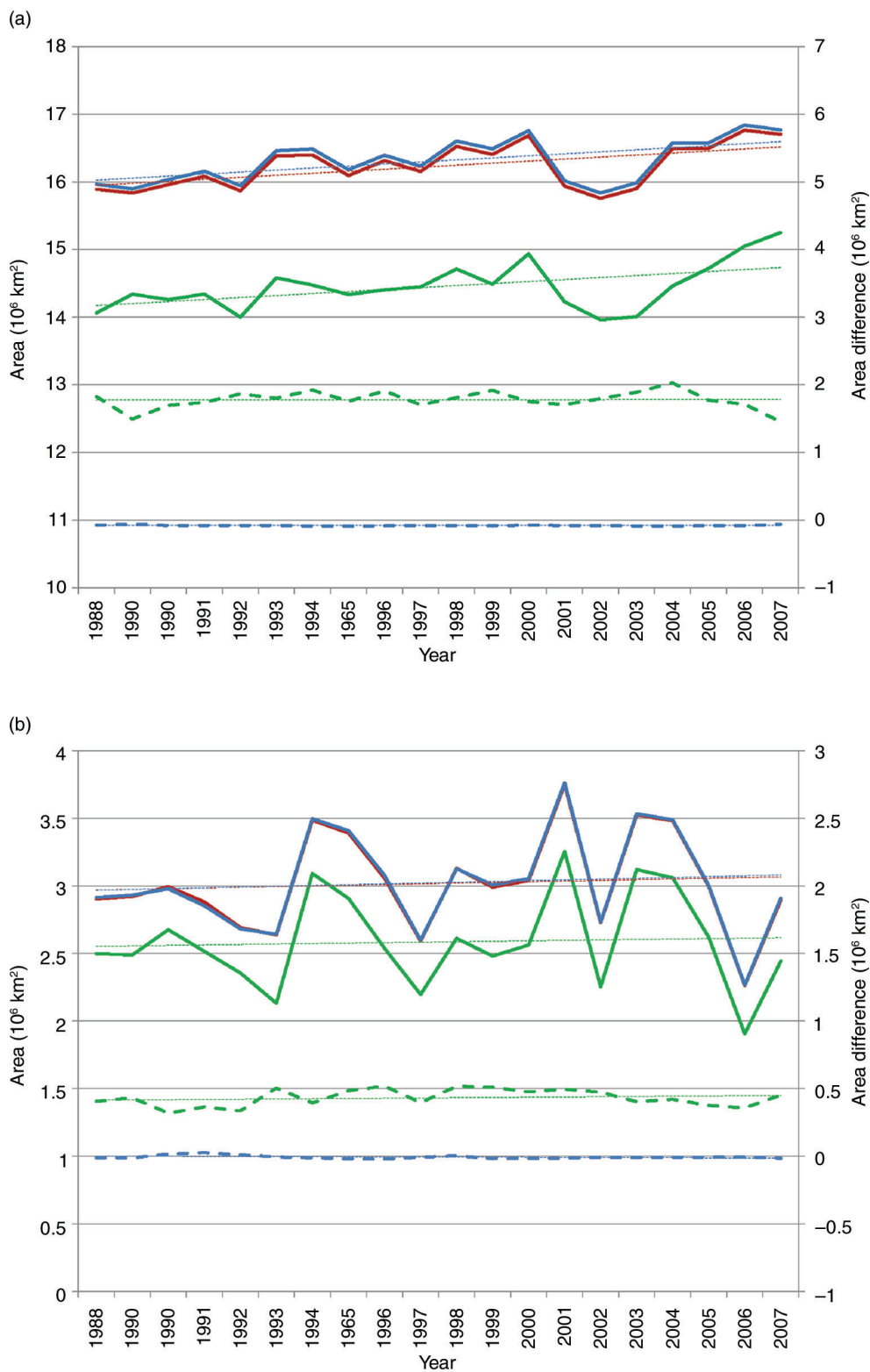
Fig. 15 Southern Hemisphere CDR ice area for (a) March and (b) September from the National Oceanic and Atmospheric Administration Climate Data Record (CDR; red), Bootstrap (blue) and NASA Team (green), in solid lines. Dashed lines are the difference between CDR and Goddard Space Flight Center. Dotted lines are linear trends.

Table 6 Monthly sea-ice extent trend estimates (in km^2) over 1988–2007 for the National Oceanic and Atmospheric Administration Climate Data Record (CDR) and the difference between CDR and NASA Team (NT) for the Northern and Southern Hemispheres.

Month	Northern Hemisphere		Southern Hemisphere	
	CDR trend	CDR–NT trend (SD)	CDR trend	CDR–NT trend (SD)
January	−59 500	−600 (94 900)	−1100	0 (97 800)
February	−49 600	−2300 (89 700)	+9500	+3100 (7000)
March	−49 500	−7000 (101 800)	−5200	+1800 (11 800)
April	−37 200	−3200 (95 500)	+5500	+1300 (9000)
May	−30 200	+1700 (92 800)	+2100	+6100 (43 200)
June	−51 300	+9400 (127 300)	+20 100	+5600 (25 100)
July	−71 500	−3000 (129 800)	+26 300	+9400 (18 100)
August	−83 700	−7500 (159 500)	+11 400	+1300 (33 000)
September	−91 700	−16 600 (178 700)	+29 800	+300 (6900)
October	−95 000	+2600 (125 200)	+24 700	+8800 (17 100)
November	−72 600	+1700 (104 900)	+15 700	+8900 (41 900)
December	−68 275	+7400 (120 100)	+15 000	−3500 (107 600)

sea-ice time series exist, but most are produced in a research mode without fully transparent processing and complete documentation. Also the products are not generally distributed and archived in a way that facilitates long-term preservation. The approach presented here was not to develop an entirely novel methodology but rather to build upon well-established passive microwave data sets and enhance them to meet the NOAA CDR requirements. The CDR product presented here does so through (1) fully automated processing with all source code available, (2) thorough documentation of the algorithm and software, (3) distribution of data in a self-describing file format (NetCDF), (4) ISO 19115-2

Table 7 Monthly sea ice extent trend estimates (in km^2) over 1988–2007 for the National Oceanic and Atmospheric Administration Climate Data Record (CDR) and the difference between CDR and Bootstrap (BT) for the Northern and Southern Hemispheres.

Month	Northern Hemisphere		Southern Hemisphere	
	CDR trend	CDR–BT trend (SD)	CDR trend	CDR–BT trend (SD)
January	−59 500	−500 (26 500)	+700	−200 (12 800)
February	−49 600	−100 (68 800)	+100	+500 (7000)
March	−49 500	−700 (38 400)	−700	−300 (11 800)
April	−37 200	−700 (40 100)	−200	+900 (9000)
May	−30 200	−800 (42 300)	−1900	−1800 (43 200)
June	−51 300	−1000 (52 600)	−1900	−1200 (25 100)
July	−71 500	−3300 (41 700)	+600	+300 (18 000)
August	−83 700	−2900 (60 400)	+600	+1300 (33 000)
September	−91 700	+400 (55 500)	−100	−300 (6900)
October	−95 000	+6100 (74 700)	+200	+3000 (17 100)
November	−72 600	+100 (30 000)	+900	+1300 (41 900)
December	−68 275	+2100 (36 300)	−8000	−5700 (108 600)

compliant collection-level metadata, (5) file-level metadata (NetCDF CF) and (6) grid cell level metadata in the form of error-indication (spatial standard deviation) and quality-assessment fields.

The CDR has been evaluated here through a variety of comparisons with the foundational sea-ice products from the GSFC. The most substantial difference is due to the fact that the CDR does not interpolate missing data. This was done to maximize transparency and to allow users to interpolate (or not) as they see fit. Other differences result from manual corrections done for GSFC that are not feasible in an automated CDR processing system. These manual corrections primarily removed false ice along Northern Hemisphere coasts due to mixed land–ocean grid cells (i.e., land-spillover due to the large sensor footprints). These differences were found to be small and comparisons between CDR and GSFC fields show close agreement. Perhaps most important for a climate record, trend estimates were nearly identical between CDR and GSFC, confirming that the CDR sea-ice concentration product is suitable for tracking climate change and variability.

This paper analyses Version 1 of the CDR product, encompassing July 1987–December 2007. The product has been updated through 2012 during spring 2013 and routine quarterly updates will follow. Enhancements are under development, including investigation of the feasibility of adding the SMMR sensor to the CDR product, if data quality issues can be managed. This would extend the CDR concentration parameter back to October 1978, matching the timespan of the GSFC products. Another potential enhancement that will be considered is spatial gap-filling missing data in the daily CDR concentration fields.

Acknowledgements

References

Agnew T. & Howell S. 2003. The use of operational ice charts for evaluating passive microwave ice concentration data. *Atmosphere–Ocean 41*, 317–331.

Andersen S., Tonboe R., Kaleschke L., Heygster G. & Pedersen L.T. 2007. Intercomparison of passive microwave sea ice concentration retrievals over the high-concentration Arctic sea ice. *Journal of Geophysical Research—Oceans 112*, C08004, doi: 10.1029/2006JC003543.

Brucker L., Cavalieri D.J., Markus T. & Ivanoff A. 2014. NASA Team 2 sea ice concentration algorithm retrieval uncertainty. *IEEE Transactions on Geoscience and Remote Sensing 52*, 7336–7352.

Cavalieri D., Parkinson C., DiGirolamo N. & Ivanov A. 2012. Intersensor calibration between F13 SSM/I and F17 SSMIS for global sea ice data records. *IEEE Geoscience and Remote Sensing Letters 9*, 233–236.

Cavalieri D., Parkinson C., Gloersen P. & Zwally H.J. 1996 (updated yearly). *Sea ice concentrations from Nimbus-7 SMMR and DMSP SSM/I-SSMIS passive microwave data. 1978–2007.* Digital media. Boulder, CO: National Aeronautics and Space Administration Distributed Active Archive Center at the National Snow and Ice Data Center. Accessed on the internet at http://nsidc.org/data/nsidc-0051.html on 1 February 2013.

Cavalieri D.J. 1994. A microwave technique for mapping thin sea ice. *Journal of Geophysical Research—Oceans 99*, 12561–12572.

Cavalieri D.J., Crawford J.P., Drinkwater M.R., Eppler D.T., Farmer L.D., Jentz R.R. & Wackerman C.C. 1991. Aircraft active and passive microwave validation of sea ice concentration from the Defense Meteorological Satellite Program Special Sensor Microwave Imager. *Journal of Geophysical Research—Oceans 96*, 21989–22008.

Cavalieri D.J., Gloersen P. & Campbell W.J. 1984. Determination of sea ice parameters with the NIMBUS-7 SMMR. *Journal of Geophysical Research—Atmospheres 89*, 5355–5369.

Cavalieri D.J. & Parkinson C.L. 2012. Arctic sea ice variability and trends, 1979–2010. *The Cryosphere 6*, 881–889.

Cavalieri D.J., Parkinson C.L., Gloersen P., Comiso J.C. & Zwally H.J. 1999. Deriving long-term time series of sea ice cover from satellite passive-microwave multisensor data sets. *Journal of Geophysical Research—Oceans 104*, 15803–15814.

Comiso J.C. 1986. Characteristics of Arctic winter sea ice from satellite multispectral microwave observations. *Journal of Geophysical Research—Oceans 91*, 975–994.

Comiso J.C. 2000 (updated 2012). *Bootstrap sea ice concentrations from Nimbus-7 SMMR and DMSP SSM/I-SSMIS. Version 2. 1978–2007.* Digital media. Boulder, CO: National Aeronautics and Space Administration Distributed Active Archive Center at the National Snow and Ice Data Center. Accessed on the internet at http://nsidc.org/data/nsidc-0079.html on 1 February 2013.

Comiso J.C., Cavalieri D., Parkinson C. & Gloersen P. 1997. Passive microwave algorithms for sea ice concentrations: a comparison of two techniques. *Remote Sensing of the Environment 60*, 357–384.

Comiso J.C. & Nishio F. 2008. Trends in the sea ice cover using enhanced and compatible AMSR-E, SSM/I, and SMMR Data. *Journal of Geophysical Research—Oceans 113*, C02S07, doi: 10.1029/2007JC0043257.

Eastwood S., Larsen K.R., Lavergne T., Nielsen E. & Tonboe R. 2011. *Global sea ice concentration reprocessing. Product user manual. Product OSI-409. Document version 1.3. Data set version 1.1.* Ocean and Sea Ice Satellite Application Facility. Accessed on the internet at http://www.osi-saf.org on 19 November 2013.

Kattsov V.M., Ryabinin V.E., Overland J.E., Serreze M.C., Visbeck M., Walsh J.E., Meier W.N. & Zhang X. 2010. Arctic sea-ice change: a grand challenge of climate science. *Journal of Glaciology 56*, 1115–1121.

Kwok R. 2002. Sea ice concentration estimates from satellite passive microwave radiometry and openings from SAR ice motion. *Geophysical Research Letters 29*, article no. 1311, doi: 10.1029/2002GL014787.

Markus T. & Cavalieri D.J. 2000. An enhancement of the NASA team sea ice algorithm. *IEEE Transactions Geoscience Remote Sensing 38*, 1387–1398.

Maslanik J. & Stroeve J. 2004 (updated 2012). *DMSP SSM/I-SSMIS daily polar gridded brightness temperatures. Version 4. 1987–2007.* Boulder, CO: National Aeronautics and Space Administration Distributed Active Archive Center at the National Snow and Ice Data Center. Accessed on the internet at http://nsidc.org/data/nsidc-0001.html on 1 February 2013.

Meier W.N. 2005. Comparison of passive microwave ice concentration algorithm retrievals with AVHRR imagery in Arctic peripheral seas. *IEEE Transactions Geoscience Remote Sensing 43*, 1324–1337.

Meier W.N. 2012. Climate algorithm theoretical basis document (C-ATBD). Passive microwave sea ice concentration. CDRP-ATBD-0107. Version 2, 29 May 2012. Asheville, NC: National Oceanic and Atmospheric Administration Climate Data Record Program.

Murphy A.H. & Winkler R.L. 1987. A general framework for forecast verification. *Monthly Weather Review 115*, 1330–1338.

NRC (National Research Council) 2004. *Climate data records from environmental satellites.* Washington, DC: National Academies Press.

Parkinson C.L. & Cavalieri D.J. 2012. Antarctic sea ice variability and trends, 1979–2010. *The Cryosphere 6*, 871–880.

Partington K., Flynn T., Lamb D., Bertoia C. & Dedrick K. 2003. Late twentieth century Northern Hemisphere sea-ice record from U.S. National Ice Center ice charts. *Journal of Geophysical Research—Oceans 108*, article no. 3343, doi: 10.1029/2002JC001623.

Partington K.C. 2000. A data fusion algorithm for mapping sea-ice concentrations from Special Sensor Microwave/Imager data. *IEEE Transactions Geoscience Remote Sensing 38*, 1947–1958.

Peng G., Meier W.N., Scott D.J. & Savoie M.H. 2013. A long-term and reproducible passive microwave sea ice concentration data record for climate studies and monitoring. *Earth System Science Data 5*, 211–318.

Steffen K., Key J., Cavalieri D.J., Comiso J., Gloersen P., St. Germain K. & Rubinstein I. 1992. The estimation of geophysical parameters using passive microwave algorithms. In F.D. Carsey (ed.): *Microwave remote sensing of sea ice*. Pp. 201–231. Washington, DC: American Geophysical Union.

Taylor K.E. 2001. Summarizing multiple aspects of model performance in a single diagram. *Journal of Geophysical Research—Atmospheres 106*, 7183–7192.

Van Woert M.L., Zou C.Z., Meier W.N., Hovey P.D. & Chase M. 2003. 24-hour forecast verification of the operational "Polar Ice Prediction System." In V. Squire & P. Langhorne (eds.): *Ice in the environment: proceedings of the 16th IAHR international symposium ice 2, Dunedin, New Zealand, 2–6 December 2002.* Pp. 445–452. Madrid: International Association of Hydraulic Engineering and Research.

Wentz F.J. 1997. A well calibrated ocean algorithm for special sensor microwave/imager. *Journal of Geophysical Research—Oceans 102*, 8703–8718.

Wentz F.J. 2010. The version-6 calibration of SSM/I. *RSS Technical report number 102210*. Santa Rosa, CA: Remote Sensing Systems.

Wilks D. 2011. *Statistical methods in the atmospheric sciences*. 3rd edn. Oxford: Academic Press.